

# Artifact Suppression in Imaging of Myocardial Infarction Using $B_1$ -Weighted Phased-Array Combined Phase-Sensitive Inversion Recovery

Peter Kellman,\* Christopher K. Dyke, Anthony H. Aletras, Elliot R. McVeigh, and Andrew E. Arai

**Regions of the body with long  $T_1$ , such as cerebrospinal fluid (CSF), may create ghost artifacts on gadolinium-hyperenhanced images of myocardial infarction when inversion recovery (IR) sequences are used with a segmented acquisition. Oscillations in the transient approach to steady state for regions with long  $T_1$  may cause ghosts, with the number of ghosts being equal to the number of segments.  $B_1$ -weighted phased-array combining provides an inherent degree of ghost artifact suppression because the ghost artifact is weighted less than the desired signal intensity by the coil sensitivity profiles. Example images are shown that illustrate the suppression of CSF ghost artifacts by the use of  $B_1$ -weighted phased-array combining of multiple receiver coils. Magn Reson Med 51: 408–412, 2004. Published 2004 Wiley-Liss, Inc.†**

**Key words:** MRI; artifact; delayed hyperenhancement; heart; myocardial infarction; phased array; cerebrospinal fluid (CSF); phase-sensitive

Myocardial viability assessment using Gd-DTPA hyperenhancement MRI is gaining clinical acceptance (1,2). With the use of recently developed MRI methods (3) myocardial infarction can be imaged with high spatial resolution and good contrast. Following administration of Gd-DTPA, infarcted myocardium exhibits delayed hyperenhancement and can be imaged with an inversion recovery (IR) sequence.

Oscillations in the transient approach to steady state for regions with long  $T_1$ , such as CSF, may cause artifacts in breath-held, segmented imaging. Unlike breathing or other motion-related artifacts, the artifacts due to CSF in the spinal column are generally small and thus are less well recognized as an artifact. This artifact mechanism is detailed in this study, and it is shown that  $B_1$ -weighted phased-array combining (4) provides an inherent suppression of this artifact, which adequately mitigates this issue.

The image reconstruction method uses phase-sensitive detection with  $B_1$ -weighted phased-array combining to optimize SNR. Phase-sensitive IR (PSIR) techniques have demonstrated a number of benefits (5), including consistent contrast and appearance over a relatively wide range of inversion times (TIs), improved contrast-to-noise ratio

(CNR), and consistent size of the hyperenhanced region. In addition to the artifact suppression provided by  $B_1$ -weighted phased-array combining, phase-sensitive reconstruction also suppresses artifacts that arise from the asymmetric  $k$ -space weighting due to IR and magnetization readout (5).

When using Gd-DTPA with an IR acquisition sequence, it is desirable to use inversion pulses every other heartbeat to achieve almost full magnetization recovery. Therefore, it is possible to acquire a low flip angle readout reference image during alternate heartbeats without increasing the breath-hold duration or decreasing the  $T_1$  contrast of the desired IR image. Cardiac imaging poses unique challenges due to the combined effects of field inhomogeneity, motion, and low SNR, which make it difficult to obtain a reliable estimate of the background phase and  $B_1$ -maps. The approach described in Ref. 5 overcomes these difficulties by acquiring a reference image at the same cardiac phase, during the same breath-hold acquisition, and during alternate heartbeats, to estimate both the background phase and surface coil field maps. This type of acquisition provides a reference image with good spatial resolution and eliminates misregistration errors due to motion.

## MATERIALS AND METHODS

### Pulse Sequence

The pulse sequence timing used in this study is diagrammed in Fig. 1. For each slice, imaging was performed in mid-diastole using a prospectively gated, segmented acquisition of  $k$ -space over several heartbeats during a single breath-hold. IR pulses were applied every other heartbeat to permit nearly full recovery of magnetization in the presence of Gd-DTPA. This minimizes any disruption of the steady-state due to heart rate variability. A reference phase map was acquired during the same breath-hold and cardiac phase in alternate heartbeats using a reduced flip angle readout. In this manner, both the IR and reference image are spatially registered, avoiding errors due to respiratory and cardiac motion. Also note that the overall imaging time was not increased by the reference acquisition, and that the reference acquisition with reduced flip angle readout resulted in only a small loss of magnetization to the IR image.

A fast gradient-recalled echo pulse sequence was used with interleaved phase-encode ordering. The inversion was performed via a nonselective, Silver-Hoult adiabatic pulse (6). The  $T_1$ -weighted IR image was acquired using multiple  $20^\circ$  flip angle pulses, while the reference used  $5^\circ$  flip angle pulses. The reference image was acquired after

Laboratory of Cardiac Energetics, National Heart, Lung and Blood Institute, National Institutes of Health, DHHS, Bethesda, Maryland.

\*Correspondence to: Peter Kellman, Laboratory of Cardiac Energetics, National Institutes of Health, National Heart, Lung and Blood Institute, 10 Center Drive, MSC-1061, Building 10, Room B1D416, Bethesda, MD 20892-1061. E-mail: kellman@nih.gov

Received 30 May 2003; revised 11 September 2003; accepted 12 September 2003.

DOI 10.1002/mrm.10689

Published online in Wiley InterScience (www.interscience.wiley.com).

Published 2004 Wiley-Liss, Inc. † This article is a US Government work and, as such, is in the public domain in the United States of America.

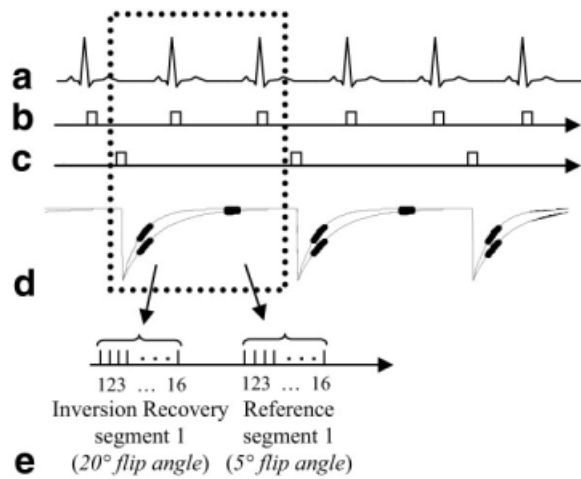


FIG. 1. Pulse sequence diagram for gated, segmented  $k$ -space acquisition of IR and reference images using low flip angle readouts. Data for IR and reference images are collected alternately every other heartbeat.

the magnetization had recovered almost completely. The use of a  $5^\circ$  flip angle for the reference image reduces the  $T_1$  contrast of the reference image, and minimizes relaxation effects on the primary  $T_1$ -weighted IR image.

The IR of magnetization plotted in Fig. 1 illustrates  $T_1$  values corresponding to normal and infarcted myocardia. The magnetization in both normal and infarcted myocardia has almost fully recovered after two heartbeats. For CSF, which has much longer  $T_1$ , the magnetization has not yet recovered. The magnetization of the CSF oscillates as it approaches steady state. This may create an artifact due to the interleaved segmented phase-encode acquisition order, as described below in greater detail.

The sequence was implemented on GE Signa CV/i and Siemens Sonata 1.5 T scanners using similar parameters. Results are provided for the GE scanner. Typical parameters for the GE scanner were as follows: bandwidth =  $\pm 31.25$  kHz, TE = 3.4 ms, TR = 7.8 ms, readout flip angle =  $20^\circ$ . The typical FOV was  $360 \text{ mm} \times 270 \text{ mm}$ , with an image matrix of  $256 \times 96$ ; thus the in-plane spatial resolution was approximately  $1.4 \text{ mm} \times 2.8 \text{ mm}$  for both the IR and the reference images (final images were interpolated to  $256 \times 192$ ,  $1.4 \text{ mm}^2$ ). The slice thickness was 8 mm. The 96 phase encodes were acquired in 12 heartbeats by collecting 16 lines of  $k$ -space per heartbeat, with 2 R-R intervals between inversion pulses. Two heartbeats of dummy readouts at the beginning of the sequence were discarded to reduce the transient during the approach to steady state. The acquisition time (segment duration) was approximately 125 ms per R-R interval, during diastasis, which is a period of relatively little motion. Both systems use a gradient crusher. The sequence implemented on the GE system does not use RF spoiling, whereas the Siemens system does (7).

#### Phase-Sensitive Reconstruction

A  $B_1$ -weighted phased-array combined phase-sensitive reconstruction method was used (5). To improve the SNR of

the image, as well as accuracy of the background phase estimate, the complex images for each coil were optimally combined (weighted sum) (4) prior to phase-sensitive detection. The phase of the reference image was removed from the  $T_1$ -weighted IR image on a pixel-by-pixel basis, and as a result the real part of the resultant image preserved the polarity of the IR signal. The spatial resolution was the same for both the reference and the  $T_1$ -weighted IR image, as previously described.

The complex weights used for phased-array combining were the complex conjugates of the estimates of relative coil sensitivities, which were normalized by the noise standard deviation for each coil. The use of relative, rather than absolute, coil sensitivities ( $B_1$ -maps) alleviated the need for separate acquisition of body coil images. The relative, complex coil sensitivities were estimated using the individual complex reference coil images, by a previously described procedure (5). By applying the same  $B_1$ -weighted complex combining to both  $T_1$ -weighted IR and reference images, any phase error in the  $B_1$ -maps was canceled in the phase-sensitive (homodyne) image.

#### Artifact Characterization

We characterized artifacts resulting from the oscillatory approach to steady state for regions with long  $T_1$  by calculating a simulated point spread function (PSF). The transverse magnetization vector for each RF readout during the transient approach to steady state was calculated (8) for the IR sequence shown in Fig. 1, using published values of  $T_1$  and  $T_2$  (9) (4.5 and 2.2 s, respectively). While there is a wide range of published values for CSF parameters, the artifact behavior is predicted (based on simulations) to be quite similar over this range. We calculated the effective  $k$ -space weighting from the magnetization for each pulse after accounting for the interleaved order of the segmented acquisition, as well as a single segment discarded acquisition. The PSF was then calculated by FFT of the  $k$ -space weighting. Normal and infarcted myocardia were simulated as well, using nominal  $T_1$  values of 390 and 250 ms, respectively, and 50 ms for  $T_2$ . The TI was set to null the normal myocardium.

Figure 2 shows the magnetization amplitude vs. the phase-encode line number ( $k_y$ ) after reordering, and the corresponding PSF for several cases. The left column is for infarcted (bold line) and normal (light line) myocardia. Figure 2a shows magnetization recovery, and Fig. 2b–d show the real, imaginary, and magnitude PSFs, respectively. The normal myocardium is approximately nulled in the center of  $k$ -space. The asymmetric  $k$ -space weighting due to IR during the segment leads to an imaginary component in the PSF. This imaginary component can cause an edge artifact in magnitude-reconstructed images. However, phase-sensitive reconstruction, which uses the real part, will not have this artifact (5). The magnetization and PSFs are plotted for CSF without RF spoiling in the right column of Fig. 2. The magnetization has an oscillatory approach to steady state that causes substantial artifacts (ghost images equal to the number of segments and evenly distributed across the FOV), which are evident in the PSFs (Fig. 2f–h). A  $20^\circ$  readout flip angle ( $5^\circ$  for reference image) was used in these simulations.

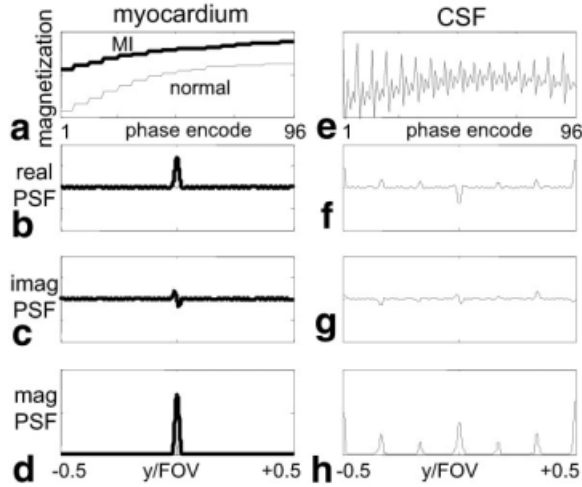


FIG. 2. Simulated magnetization recovery and corresponding PSFs for segmented acquisition with interleaved phase order. Normal and infarcted (bold) myocardia are shown in **a–d**, and CSF is shown in **e–h**. The transient approach to steady state for CSF with long  $T_1$  causes ghost artifacts.

### Artifact Suppression

Although  $B_1$ -weighted phased-array combining is used primarily to optimize the SNR, it also provides a degree of artifact suppression (4), particularly for artifacts with wide ghost spacing (e.g.,  $FOV/2$ ). An expression for the individual coil images with ghost artifact may be written as:

$$g_i(x, y) = s_i(x, y)f(x, y) + h(D)s_i(x, y + D)f(x, y + D) \quad [1]$$

where  $i$  is the coil index,  $s_i(x, y)$  is the complex coil sensitivity profile,  $f(x, y)$  is the desired image with  $T_1$  contrast,  $D$  is the ghost separation distance (e.g.,  $FOV/2$ ), and  $h(D)$  is the value of the PSF for this ghost. The root-sum-of-squares (RSS) magnitude combined image is given by:

$$mag_{RSS} = \sqrt{\sum_i |g_i(x, y)|^2} \quad [2]$$

and the magnitude of the  $B_1$ -weighted phased-array combined image as:

$$mag_{B1-wt} = \left| \sum_i g_i(x, y)s_i^*(x, y) \right| \quad [3]$$

where  $*$  corresponds to the complex conjugate. Magnitude rather than phase-sensitive detection is used in Eq. [3] in order to derive a simple expression for artifact suppression due to the phased-array combining alone. To further simplify the expression for artifact suppression, consider the case where  $f(x, y)$  corresponds to normal myocardium, which is assumed to be nulled. In this case,  $f(x, y) = 0$  and  $f(x, y + D)$  is the CSF signal. For this case, the artifact suppression is simply the ratio

$$\rho = \frac{mag_{B1-wt}}{mag_{RSS}} = \frac{\left| \sum_i s_i(x, y + D)s_i^*(x, y) \right|}{\sqrt{\sum_i |s_i(x, y + D)|^2}} \quad [4]$$

An experimental measurement of the artifact suppression due to  $B_1$ -weighted phased-array combining was derived by evaluating the expression in Eq. [4] using the magnitude values of  $B_1$ -map estimates at the artifact location and source of artifact (in this example, the spinal cord).

### Experimental Parameters

Delayed hyperenhancement images are routinely acquired by this method in patients with suspected coronary disease under two clinical research protocols approved by the Institutional Review Board of the National Heart, Lung, and Blood Institute, with prior informed consent. The hyperenhancement imaging protocol consists of acquiring a stack of short-axis slices (typically eight slices), as well as several long-axis slices (typically three slices). Images are usually acquired 10–30 min after a double dose (0.2 mmol/kg) of contrast agent (Gadopentetate Dimeglumine, Berlex Magnevist) is administered. Experiments were conducted with GE Signa CV/i 1.5T and Siemens Sonata MRI systems. For the GE system, a four-element cardiac phased array (standard GE product coil) was used. This array consisted of two pairs of overlapped, rectangular coils (19 cm  $\times$  11.5 cm, with the long dimension oriented along the S/I direction and a 2-cm overlap in the L/R direction), with one pair positioned on the chest, and the second pair positioned on the back of the patient. For the Siemens system, a custom eight-element cardiac phased array (Nova Medical, Inc., Wakefield, MA) was used. This array consisted of two four-element gapped linear arrays (22 cm  $\times$  5.25 cm element size, with the long dimension oriented along the S/I direction, and a  $\sim$ 1.25 cm gap in the L/R direction), with one array positioned on the chest, and the second array positioned on the back of the patient. Magnitude and phase-sensitive IR images were reconstructed for each study. Raw data were acquired for each study, which allowed retrospective reconstruction of individual coil images.

### RESULTS

Long-axis images of the heart acquired using the GE system are shown to illustrate the artifact suppression achieved using  $B_1$ -weighted phased-array combining. The artifact is more prevalent in the four-chamber view. Images from the GE system reconstructed using both RSS magnitude combining and  $B_1$ -weighted phased-array combined phase-sensitive reconstruction are shown in Fig. 3a and b, respectively. Magnitude and phase-sensitive images were acquired using the same breath-hold data, as previously described above. In this case, the normal myocardium was nulled at approximately 300 ms; however, an artifact may be observed in the magnitude image that is not present in the  $B_1$ -weighted phased-array combined phase-sensitive image, which was reconstructed using the same data. The magnitude images for the individual coils are shown in

FIG. 3. Long-axis delayed hyper-enhancement images illustrating (a) artifact in an RSS magnitude combined IR image, and (b) suppressed artifact in a  $B_1$ -weighted phased-array combined PSIR image.

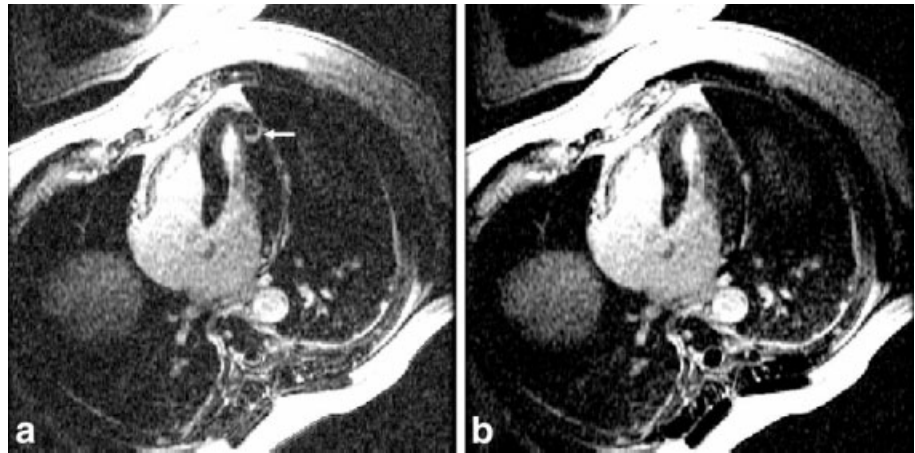


Fig. 4. The artifact is clearly caused by ghosting of the CSF in the spinal cord, and is only evident in the back coils (Fig. 4c and d). In vivo estimates of the  $B_1$  maps derived from the reference images after almost complete magnetization recovery are shown in Fig. 5. The CSF artifact is suppressed by the  $B_1$  weighting. The suppression was calculated using Eq. [4] to be approximately  $\rho = 0.25$  for  $D = \text{FOV}/2$  (suppressed 4:1).

## DISCUSSION

A CSF ghost artifact was evident in segmented IR sequences used to image myocardial infarction on both GE and Siemens (not shown) systems. The  $B_1$ -weighted phased-array combining adequately suppressed the artifact in both cases. The Siemens implementation used RF spoiling. Analyses of the transient approach to steady state for RF spoiling are typically given for continuous RF pulses, whereas in this segmented acquisition there is

considerable interruption of the steady state between segments, as well as inversion pulses applied every two segments. The use of RF phase spoiling in this segmented acquisition with  $T_1$  on the order of two consecutive phase encodes (segments) was found to reduce, but not eliminate, the CSF artifact. Therefore, the artifact suppression provided by the  $B_1$ -weighted phased-array combining was important.

Since the ghosts appear in the phase-encode direction, one could also resolve the artifact by swapping the frequency and phase-encode directions or using an in-plane rotation. While this approach may be useful during the scan (at the expense of additional breath-hold), it is only effective if the artifact is immediately identified, which depends on the skill of the operator. The CSF artifact is rather small, unlike larger breathing or motion-related artifacts, and is less well recognized as an artifact. In the example shown in Fig. 3a, the patient had a history of sarcoidosis. In this case a hyperenhanced region, which is not subendocardial and resembles the CSF artifact, might suggest cardiac involvement. Failure to resolve this case could have resulted in a misdiagnosis.

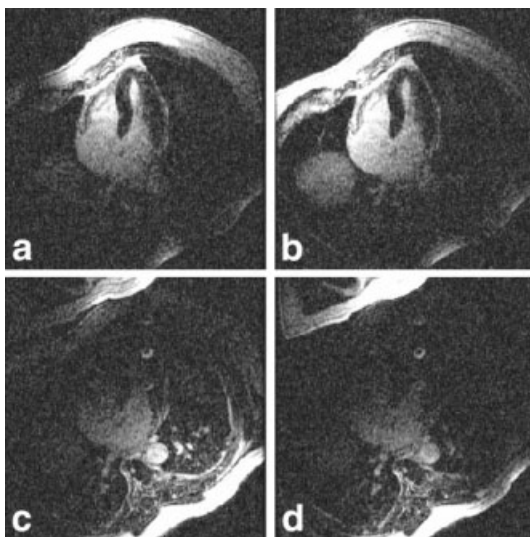


FIG. 4. Magnitude images for individual coils illustrating  $B_1$  weighting of ghost artifacts. The artifact from CSF in the spinal cord is evident in images from the back coils (c and d), and is suppressed in chest coil images (a and b).

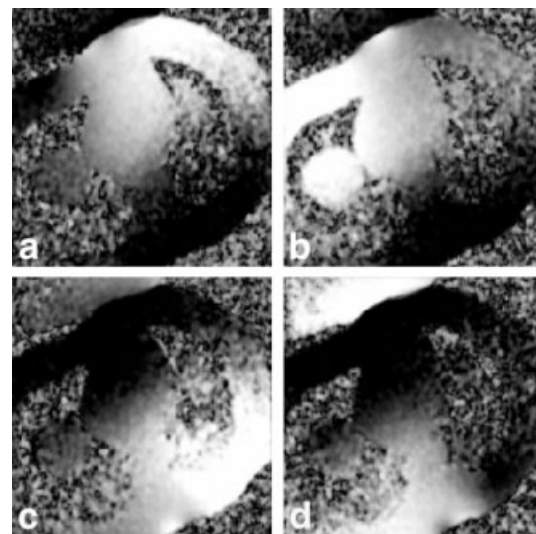


FIG. 5. Magnitude of in vivo estimates of  $B_1$  maps for a four-element cardiac phased array.

CSF ghost artifacts were not evident in the in vivo  $B_1$ -map estimates, for several reasons. The reference images are acquired with a reduced flip angle readout after the magnetization is almost recovered, so that the intensities are almost proton density-weighted with little  $T_1$  contrast. Furthermore, there is a significantly reduced transient during the approach to steady state. Therefore, the blood and myocardial signals are stronger than the CSF signal. Additionally, the  $B_1$ -map estimates use spatial smoothing, which further reduces any contribution due to a small artifact structure.

The effectiveness of  $B_1$ -weighted phased-array combining in suppressing artifacts depends on the coil sensitivity roll-off, with greater suppression for smaller coils. The cardiac surface coil arrays used for this application were well suited for this purpose. Larger torso coils may not have enough roll-off to provide adequate artifact suppression for FOV/2 ghosts.

## CONCLUSIONS

Hyperenhancement imaging of myocardial infarction using IR sequences with a breath-held, segmented acquisition may lead to an artifact in regions with long  $T_1$  (such as CSF) due to oscillations in the transient approach to steady state.  $B_1$ -weighted phased-array combined phase-sensitive

reconstruction provides an inherent degree of artifact suppression that is shown to effectively mitigate this artifact.

## REFERENCES

1. Kim RJ, Fieno DS, Parrish TB, Harris K, Chen EL, Simonetti O, Bundy J, Finn JP, Klocke FJ, Judd RM. Relationship of MRI delayed contrast enhancement to irreversible injury, infarct age, and contractile function. *Circulation* 1999;100:1992–2002.
2. Kim RJ, Wu E, Rafael A, Chen EL, Parker MA, Simonetti O, Klocke FJ, Bonow RO, Judd RM. The use of contrast-enhanced magnetic resonance imaging to identify reversible myocardial dysfunction. *N Engl J Med* 2000;343:1445–1453.
3. Simonetti OP, Kim RJ, Fieno DS, Hillenbrand HB, Wu E, Bundy JM, Finn JP, Judd RM. An improved MR imaging technique for the visualization of myocardial infarction. *Radiology* 2001; 218:215–223.
4. Roemer PB, Edelstein WA, Hayes CE, Souza SP, Mueller OM. The NMR phased array. *Magn Reson Med* 1990;16:192–225.
5. Kellman P, Arai AE, McVeigh ER, Aletras AH. Phase sensitive inversion recovery for detecting myocardial infarction using gadolinium delayed hyperenhancement. *Magn Reson Med* 2002;47:372–383.
6. Silver MS, Joseph RI, Hoult DI. Highly selective  $PI/2$  and  $PI$ -pulse generation. *J Magn Reson* 1984;59:347–351.
7. Crawley AP, Wood ML, Henkelman RM. Elimination of transverse coherences in FLASH MRI. *Magn Reson Med* 1988;8:248–260.
8. Sekihara K. Steady-state magnetizations in rapid NMR imaging using small flip angles and short repetition intervals. *IEEE Trans Med Imaging* 1987;6:157–164.
9. Haacke EM, Brown RW, Thompson MR, Venkatesan R. *Magnetic resonance imaging: physical principles and sequence design*. New York: John Wiley & Sons; 1999. p 54.